Penerbit Akademia Baru

Journal of Research in Nanoscience and Nanotechnology

Journal homepage:
http://akademiabaru.com/submit/index.php/jrnn/index
ISSN: 2773-6180

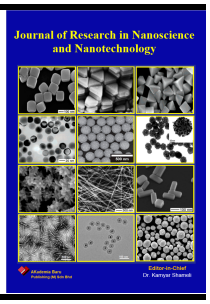

Magnetic Field and Heat Generation Effects on the Squeezing Williamson Hybrid Nanofluid Flow between Two Parallel Plates

Nurhanny Izlya Mohammad Fauzi [1], Mohd Ariff Admon [2] and Yasser Salah Hamed [2,*]

[1] Department of Mathematics, Faculty of Science, Universiti Teknologi Malaysia, 81310 Skudai, Johor, Malaysia
[2] Department of Mathematics and Statistics, Faculty of Science, Taif University, El- Haweiah, Saudi Arabia

* Correspondence: ariffadmon@utm.my
https://doi.org/10.37934/jrnn.16.1.2637

ABSTRACT

The current study intends to discuss on the effects of heat and magnetic fields on the squeezing of Williamson fluid between two parallel plates that compromises the magnetic hydrodynamic, thermal reaction, suction/injection of the hybrid nanofluid flow. The study focuses on non-Newtonian Williamson fluid comprising of ethylene glycol $C_2H_6O_2$ with two types of nano particles, copper and aluminium oxide $[Cu - Al_2O_3]$. Model involving two-dimensional, incompressible parallel plates are considered in this study. Dimensionless ODE transmitted from modelled expressions are utilized from several established transformations, then solved numerically using bvp4c algorithm in MATLAB software. Validation of the results is then being compared with the previously published research data which brings the data into an agreement. The impact of various physical parameters is analysed through plots and tables. The numerical results reveal that intensifying the squeezing parameter accelerates fluid compression, thereby elevating skin-friction while simultaneously augmenting the Nusselt number owing to steeper temperature gradients near the walls. A stronger transverse magnetic field, on the other hand, induces a Lorentz drag that effects the axial velocity, thickens the hydrodynamic boundary layer, and diminishes convective heat transfer. Suction at the plates is shown to stabilise the boundary layer and enhance cooling efficiency, whereas injection produces the opposite trend. Increasing the Williamson parameter that attenuates viscoelastic resistance, lowers shear stress, and modestly raises the Nusselt number. The hybrid nanoparticle pair of Cu and Al_2O_3 markedly boosts thermal conductivity relative to mono-nanofluids, offsetting the adverse thermal effects of magnetic damping and internal heat generation.

Keywords:
Williamson hybrid nanofluid; Squeezing flow; Parallel Pates

Received: 15 July 2025 | **Revised: 30 July 2025** | **Accepted: 21 August 2025** | **Published: 25 August 2025**

1. Introduction

Fluids can be classified into Newtonian and non-Newtonian categories based on their rheological behaviour. Newtonian fluids such as alcohol, motor air and water exhibit a linear relationship between shear rate and strain rate as described by Newton's law of viscosity [1]. However, for non-Newtonian fluid such as the Williamson fluid, it is particularly significant due to the shear-thinning properties that makes it a good fluid to function under various conditions [2]. Non-Newtonian fluid has gained significant importance due to the inherent limitations of the Newtonian fluids in various mechanical applications [3].

The relationship between magnetic field and heat generation effect on the non-Newtonian fluids causes a complex phenomenon on the boundary layer due to Lorentz force and altered thermal performance [4],[5]. The study of nanofluid particles has gained researchers attention due to the enhanced thermal properties which is beneficial in the application of electronic cooling [6]. This is due to the types of nanoparticles that are compounded in the base fluid which results in superior thermal conductivity exhibited by the hybrid nanofluid particles in comparison to conservative nanofluid [7]. In this study, nanoparticles used are being analysed for its behaviour under the magnetohydrodynamic (MHD) squeezing flow between two parallel plates. This paper intends to fill the research gaps in the analysis of MHD squeezing flow of Williamson hybrid nanofluid flow [8].

Studies have been conducted to study the behaviour of Williamson fluid under various conditions [3]. However limited research has been done that focused on the effect of magnetic field and the heat generation effects on non-Newtonian fluids [9]. Thus, the primary objective intends to discuss the magnetic field and heat generation effect on the squeezing Williamson hybrid nanofluid flow between two parallel plates.

Firstly, governing equation will be utilized to obtain the mathematical model for this problem. This study uses copper and aluminium oxide nanoparticles in ethylene glycol as the base fluid where the effects of magnetic field and heat generation were investigated on the fluid flow [6]. Then, partial differential equation (PDEs) transformed into dimensionless ordinary differential equations (ODEs) and is solved using the bvp4c algorithm is MATLAB software. Existing research are used to validate the numerical results obtained by comparing skin friction coefficients and Nusselt number with previously published data [10].

When fluid is being compressed between two surfaces, it is known as squeezing flow which is commonly encountered in hydraulic machinery and lubrication systems [5]. It is crucial to understand the combined effects of suction/injection, thermal radiation and magnetic effects to optimize the industrial processes. In this research, the effects of magnetic field and heat transfer is discussed [9].

This research focused on the effects of various key parameters such as squeezing number Sq, magnetic field M, suction/injection parameter S,stretching/shrinking parameter λ,heat source/sink Q and nanoparticle concentration on velocity profiles and temperature distribution. Results obtained have revealed that increase in Sq, λ, M and We will raise the temperature profile while increase in S leads to decrease in the velocity profile [2]. When value of We increases, inertial forcer from squeezing effect will dominate over the magnetic resistance thus reducing the impact of Lorents force's impact [3]. This study lays a foundation for designing a complex thermal management system, turbulent regimes. By integrating rheology, nanotechnology and magnetism, this research exemplifies how fluid mechanics can solve real-world problems [1].

2. Mathematical Formulation

2.1 Governing Equations

Consider a two-dimensional, incompressible, magnetohydrodynamic (MHD) squeezing flow of Williamson hybrid nanofluid between two parallel plates. The upper plate at $y = h(t) = \sqrt{\frac{\nu_f(1-\alpha t)}{b}}$ and lower plate situated at $y = 0$. The upper plate and lower plate can move simultaneously, stretch with velocity of $v_h = \frac{-\alpha}{2}\sqrt{\frac{\nu_f}{b(1-\alpha t)}}$. The temperature are maintained at a fixed values represented by T_1 and T_2 while taking into account the possibility of fluid suction/injection at the lower plate, $v_w = \frac{-V_0}{1-\alpha t}$ where $v_0 > 0$ represents suction and $v_0 < 0$ represents injection. Linear velocity at lower stretchable plate denotes $u_w = \frac{bx}{1-\alpha t}$. Magnetic field strength is applied perpendicularly where $B(t) = \frac{B_0}{\sqrt{1-\alpha t}}$ at the lower plate. The governing conservation equations are as follows:

$$\frac{\partial u}{\partial x} + \frac{\partial v}{\partial y} = 0 \tag{1}$$

$$\frac{\partial V}{\partial t} + u\frac{\partial V}{\partial x} + v\frac{\partial V}{\partial y} = \frac{\mu_{hnf}}{\rho_{hnf}}\frac{\partial^2 V}{\partial y^2} + \sqrt{2}v_f\Gamma\frac{\partial V}{\partial y}\frac{\partial^2 V}{\partial y^2} - \frac{\sigma_{hnf}}{\rho_{hnf}}B(t)^2 V \tag{2}$$

$$\frac{\partial T}{\partial t} + u\frac{\partial T}{\partial x} + v\frac{\partial T}{\partial y} = \frac{k_{hnf}}{(\rho c_p)_{hnf}}\left(\frac{\partial^2 T}{\partial x^2}\right) + \frac{Q^*}{(\rho c_p)_{hnf}}(T - T_0) \tag{3}$$

where, $V = \frac{\partial v}{\partial x} - \frac{\partial u}{\partial y}$. The associate boundary conditions at the lower plate and upper plate are [11]:

$$u = \lambda\frac{bx}{1-\alpha t}, v = \frac{-V_0}{1-\alpha t}, T = T_1 \; at \; y = 0, u = 0, v = \frac{dh(t)}{dt}, T = T_2 \; at \; y = h(t). \tag{4}$$

Here, u and v represent velocity on the x and y direction respectively while T denotes temperature of hybrid nanofluid. Dynamic viscosity and density of hybrid nanofluid is denoted by μ_{hnf} and ρ_{hnf} respectively. Williamson parameter is denoted by W and σ_{hnf} represents the electrical conductivity of the hybrid nanofluid. $B(t)$ represents the magnetic field strength and thermal conductivity is expressed as k_{hnf} of the hybrid nanofluid. $(\rho c_p)_{hnf}$ represents the heat capacity of hybrid nanofluid. Hence, T_0 represents the reference temperature whilst Q^* represents the coefficient of heat source/sink. This research involves immersing nanoparticles of copper and aluminium oxide into Williamson hybrid nanofluid $(Cu - Al_2O_3/C_2H_6O_2)$. Table 1 shows the correlations of various properties that include dynamic viscosity, hybrid nanofluid, density, heat capacity, electrical conductivity and thermal conductivity. The correlations in Table 1 and thermophysical properties in Table 2 of both base of the fluid are referred from [13] to ensure accuracy of the results as shown below.

Table 1
Correlations of hybrid nanofluid.

Properties	**Hybrid Nanofluid**
Dynamic viscosity	$\mu_{HNF} = \frac{\mu_F}{(1-\varphi_1)^{2.5}(1-\varphi_2)^{2.5}}$
Density	$\rho_{HNF} = (1-\varphi_2)[(1-\varphi_1)\rho_F + \varphi_1\rho_{S1}] + \varphi_2\rho_{S2}$
Heat capacity	$(\rho C_P)_{HNF} = (1-\varphi_2)[(1-\varphi_1)(\rho C_P)_F + \varphi_1(\rho C_P)_{S1}] + \varphi_2(\rho C_P)_{S2}$

Electrical conductivity	$\frac{\sigma_{HNF}}{\sigma_{NF}} = \frac{\sigma_{S2} + 2\sigma_{NF} - 2(\sigma_{NF} - \sigma_{S2})\varphi_2}{\sigma_{S2} + 2\sigma_{NF} + \varphi_2(\sigma_{NF} - \sigma_{S2})}, \frac{\sigma_{NF}}{\sigma_F} = \frac{\sigma_{S1} + 2\sigma_{NF} - 2(\sigma_{NF} - \sigma_{S1})\varphi_2}{\sigma_{S1} + 2\sigma_{NF} + \varphi_1(\sigma_{NF} - \sigma_{S1})}$
Thermal conductivity	$\frac{k_{HNF}}{k_{NF}} = \frac{k_{S2} + 2k_{NF} - 2(k_{NF} - k_{S2})\varphi_2}{k_{S2} + 2k_{NF} + (k_{NF} - k_{S2})}, \frac{k_{NF}}{k_F} = \frac{k_{S1} + 2k_{NF} - 2(k_F - k_{S1})\varphi_1}{k_{S1} + 2k_F + (k_F - k_{S1})\varphi_1}$

Table 2
Thermophysical properties of base fluid and nanoparticles.

Thermophysical properties	**Ethylene Glycol** $C_2H_6O_2$	**Aluminium Oxide** Al_2O_3	**Copper** Cu
$\rho(Kg/m^3)$	1115	3970	8933
$C_p(JK/Kg)$	2430	765	385
$\sigma(s/m)$	1.10×10^{-4}	3.69×10^{7}	5.96×10^{7}
$k(W/mK)$	0.253	40	400

2.2 Similarity Transformation

To transform the dimensional partial differential equations (PDEs) into nondimensional ordinary differential equations (ODEs), the utilization of the following dimensionless variables as described is utilized by Yasmin et al.,[13].

$$\psi = \sqrt{\frac{b\nu_f}{1-\alpha t}} x f(\eta),\ u = \frac{bx}{1-\alpha t} f'(\eta),\ v = -\sqrt{\frac{b\nu_f}{1-\alpha t}} f(\eta),\ \eta = y\sqrt{\frac{b}{\nu_f(1-\alpha t)}}, \theta(\eta) = \frac{T-T_0}{T_2-T_0}, \quad (5)$$

Where T_0 represents the temperature of hybrid nanofluid flow. Next is the substitution of equation(5) into equations (2), (3) and (4), ODEs and boundary conditions are:

$$f^{iv}\frac{\mu_{hnf}/\mu_f}{\rho_{hnf}/\rho_f} - (1 - We\, f''') - f'f'' + ff''' - \frac{Sq}{2}(3f'' + \eta f''') - \frac{\sigma_{hnf}/\sigma_f}{\rho_{hnf}/\rho_f} M^2 f'' = 0. \quad (6)$$

$$\frac{1}{Pr}\left(\frac{k_{hnf}/k_f}{(\rho c_p)_{hnf}/(\rho c_p)_f}\right)\theta'' + f\theta'' - \frac{Sq}{2}\eta\theta' + \frac{Q\theta}{(\rho c_p)_{hnf}/(\rho c_p)_f} = 0. \quad (7)$$

$$f'(0) = \lambda, f(0) = S, \theta(0) = \delta, \quad (8a)$$

$$f'(1) = \lambda, f(1) = \frac{Sq}{2}, \theta(1) = 1. \quad (8b)$$

$\lambda < 0$ indicates shrinking and $\lambda > 0$ indicates stretching, $\lambda = 0$ represents fixed position of the lower plate. Dimensionless parameters of the hybrid nanofluid include Prandtl number Pr, squeezing parameter Sq, heat source/sink parameter Q, temperature ratio parameter δ, magnetic parameter M and suction/injection parameter S which are defined as followed:

$$Pr = \frac{\nu_f}{k_f/(\rho c_p)_f},\ Sq = \frac{a}{b},\ Q = \frac{Q^*}{(\rho c_p)_f}\frac{1-\alpha t}{b}, \delta = \frac{(T_1-T_0)}{(T_2-T_0)},\ M = \frac{\sigma_f \beta_0^2}{b\rho_f},\ S = \frac{V_0}{bh}.$$

Physical Quantities

The physical quantities of interest under consideration are the skin friction coefficient and the Nusselt number are defined by [13].

$$C_{fx} = -\frac{\mu_{hnf}\left(\frac{\partial u}{\partial y} + \frac{\Gamma}{2}\left(\frac{\partial u}{\partial y}\right)^2\right)_{y=0}}{\rho_F U_W^2}, \quad (9)$$

$$N_{u_x} = \frac{k_{hnf} x \left(\frac{\partial T}{\partial y}\right)_{y=0}}{k_f (T_f - T_\infty)} \quad (10)$$

Substituting equation (5) into equations (9) and (10), then the skin friction coefficient and Nusselt number at the lowest and upper plates are,

Lower: $Cf_x Re_x^{\frac{1}{2}} = \lambda_2 (f''(0) + Wef''(0)^2)$, (11a)

Upper: $Cf_x Re_x^{\frac{1}{2}} = \lambda_2 (f''(1) + Wef''(1)^2)$, (11b)

Lower: $N_{u_x} Re_x^{-\frac{1}{2}} = -\left(\frac{k_{hnf}}{k_f}\right)\theta'(0)$, (12a)

Upper: $N_{u_x} Re_x^{-\frac{1}{2}} = -\left(\frac{k_{hnf}}{k_f}\right)\theta'(1)$. (12b)

Respectively, where $Re_x = \frac{xU_w}{v_f}$, $We = \frac{\Gamma bx}{2(1-\alpha t)}\sqrt{\frac{b}{v_{f(1-\alpha t)}}}$, $\lambda_2 = \frac{\mu_{hnf}}{\mu_f}$.

3. Numerical Computation and Validation

Equations (6), (7) and (8) are solved using the bvp4c solver in MATLAB. This problem is solved using bvp4c to convert the ordinary differential equations, ODEs into a system of first-order ODEs by introducing new variables.

$(y1, y2, y3, y4, y5, y6) = (f, f', f'', f''', \theta, \theta')$. (13)

Hence, equations (6), (7) and (8) are represented as,

$$f^{iv} = \left(\frac{\rho_{hnf}/\rho_f}{\mu_{hnf}/\mu_f}\right)(1 - We\, f''')\left[\frac{Sq}{2}(3y3 + \eta y4) + \left(\frac{\sigma_{hnf}/\sigma_f}{\rho_{hnf}/\rho_f}\right)M^2 y3 + y2y3 - y1y4\right], \quad (14)$$

$$\theta'' = Pr\left(\frac{(\rho c_p)_{hnf}/(\rho c_p)_f}{k_{hnf}/k_f}\right)\left[\frac{Sq}{2}\eta y6 - y1y6 - Q\left(\frac{1}{(\rho c_p)_{hnf}/(\rho c_p)_f}\right)y5\right], \quad (15)$$

subject to boundary conditions,

$ya2 = \lambda, \quad ya1 = S, \quad ya5 = \delta,$ (16a)

$yb2 = 0, \quad yb1 = \frac{Sq}{2}, \quad yb5 = 1$, (16b)

Where ya and yb represents the lower and upper plates of the boundary conditions respectively. The appropriate value for step size of $\Delta\eta = 0.01$ and η_∞=1.

Numerical results of skin friction coefficient are compared to previously published data to verify the effectiveness of the bvp4c algorithm from MATLAB software. Table 3 and 4 shows the comparison of the skin friction coefficient at both lower and upper plates with various values of M and S.

Table 3

omparison of values of lower plate, $-\left(\frac{\mu_{hnf}}{\mu_f}\right)(1 - We)f''''(0)$ with $Pr = 6.0, Sq = \delta = 0, \lambda = 1, \phi_1 \to 0, \phi_2 \to -\infty, We \to \infty, Q = 0$, with various values of M and S.

M	S	$-\left(\frac{\mu_{hnf}}{\mu_f}\right)(1 - We)f''''(0)$		
		Present	**[11]**	**[12]**
0	0.5	7.411153	7.411153	7.411153
1	0.5	7.591618	7.591618	7.591618
4	0	4.587891	4.587891	4.587891

4	0.3	6.665662	6.665662	6.665662
4	0.5	8.110334	8.110334	8.110334
4	0.6	8.851444	8.851444	8.851444
4	1.0	11.948584	11.948584	11.948584
9	0.5	8.910096	8.910096	8.910096

Table 4
Comparison of values of upper plate, $(\mu_{hnf}/\mu_f)(1-We)f''''(0)$ with $Pr = 6.2,\ Sq = \delta = 0,\ \lambda = 1,\ \phi_1 \to 0,\ \phi_2 \to -\infty,\ We \to \infty,\ Q = 0$, with various values of M and S.

M	S	$\left(\frac{\mu_{hnf}}{\mu_f}\right)(1-We)f''''(0)$		
		Present	**[11]**	**[12]**
0	0.5	4.713303	4.713303	4.713303
1	0.5	4.739017	4.739017	4.739017
4	0	1.842447	1.842447	1.842447
4	0.3	3.653695	3.653695	3.653695
4	0.5	4.820251	4.820251	4.820251
4	0.6	8.851444	8.851444	8.851444
4	1.0	7.593426	7.593426	7.593426
9	0.5	4.964870	4.964870	4.964870

4. Results and discussion

4.1 Velocity and Temperature Profiles

The impacts of physical parameters such as non-Newtonian Williamson parameter We, squeezing number Sq, suction/injection parameter λ, magnetic parameter M and heat source/sink parameter Q on the velocity profile $f'(n)$ and temperature profile $\theta(\eta)$ of fluid flow are analysed with respect to other parameters. Figures 2a to 7b represents the analysis of parameter effects on hybrid nanofluid with different parameter values. Consequently, parameters are set as follows; $Pr = 6.2,\ Sq = 1,\ S = 0.5\ \ \lambda = 1, \phi_1 = \phi_2 = 0.01, Q = 0,\ M = 9$. Hence for We case will be considered where $We = 1.0$ represents Williamson hybrid nanofluid.

Figure 2a depicted the velocity profile $f'(\eta)$, across various Williamson parameter We of the fluid flow. As We increases from 0 to 1.0, the velocity decreases at the lower plate $\eta < 0.40$ region whereas it increases near the upper plate region $\eta > 0.40$ This indicates that a higher value of the Williamson parameter We intensifies the shear-thinning behavior of the fluid, which increases the resistance to flow in the core region between the plates. Therefore, the velocity near the upper plate increases with higher We due to this squeezing effect. Figure 2b showed the influence of the Williamson parameter We on the temperature profile $\theta(\eta)$. As We increases, a decrease in the fluid temperature is observed throughout the plates. This occurs because a higher value of We enhances the viscosity of the fluid.

In Figure 3a, the impact of squeezing number Sq is discussed for three different values of We, on the velocity profile. As Sq increases for all the values of We, the velocity of fluid also increases. When

plates move apart at $Sq < 0$, indicates that fluid will respond freely to the non-Newtonian effects from the widely spaced conditions which indicates weak squeezing effect. However, as $Sq > 0$ moves closer together, it leads to increase in fluid velocity due to the strong squeezing conditions where fluid accelerates more due to intense compression causing less significant We effect. Figure 3b observed the effect of squeezing number Sq on the temperature profile. With the increasing value of Sq, fluid temperature decreases near the lower plate at $\eta < 0.65$ while it increases near the upper plate at $\eta > 0.65$ for three different Williamson values. Due to the greater kinetic energy.

The impact of suction/injection parameter S on the velocity profile $f'(\eta)$ is shown in Figure 4a. $S < 0$ represented injection and $S > 0$ represents suction. $S < 0$ increases fluid velocity near the wall thus promoting separation of boundary layer with higher magnitude while $S > 0$ reduces fluid velocity near the wall thus enhances momentum preservation in the boundary layer, preventing separation at the boundary layer. In Figure 4b, behaviour of temperature profile $\theta(\eta)$ is illustrated. From the graph, temperature of fluid increases simultaneously with different values of We which indicates that temperature for suction is higher compared to injection.

Figure 5a illustrated the impact of various shrinking/stretching parameter λ on the velocity $f'(\eta)$. $\lambda < 0$ represents the shrinking at the lower plate while $\lambda > 0$ signifies stretching of the lower plate. At $\eta < 0.3$, velocity accelerates due to the plate's motion while simultaneously decelerating after $\eta > 0.3$. From the various values of Williamson parameter, higher We amplifies the near-wall momentum due to the shear-thinning behaviour resulting in flatter velocity distribution. Figure 5b represented the effect of temperature profile $\theta(\eta)$ with various values of λ. As lambda increases, it is observed that there is a consistent increase in temperature for all values of We due to elevated fluid temperature.

Figure 6a illustrated the impact of various magnetic parameter M on the velocity $f'(\eta)$. The increase values of M results into the decrease of velocity near the lower plate for various values of We. When $\eta > 0.45$, the velocity increases simultaneously with the magnetic parameter M due to the Lorentz force opposition. When a strong magnetic field is exerted, significant decrease is observed in the lower plate of the fluid flow. The upper plate is not affected by the magnetic field since it is only applied on the lower plate. Figure 6b observed the effects of magnetic parameter M on the temperature profile $\theta(\eta)$. For all three different values of We, value of M increases. However, decreasing the temperature distribution across boundary plates of fluid.

Figure 7a analysed the behaviour of the velocity profile $f'(\eta)$ with various values of heat source/sink parameter Q. Heat sink is indicated by $Q < 0$. Hence, $Q > 0$ indicates heat source. From the figure, for lower values of Q at $\eta < 0.4$, velocity of fluid accelerates near the wall and at $\eta > 0.5$, fluid decelerates away from the wall due to contraction of cooled fluid. For higher values of Q, at $\eta < 0.4$, velocity increases as heated fluid expands outward causing gradient to become Figure 7b showed the impact of heat source/sink on the temperature profile, $\theta(\eta)$. When $Q > 0$, thermal boundary layer thickens due to expansion of fluid which causes temperature profile to increase.

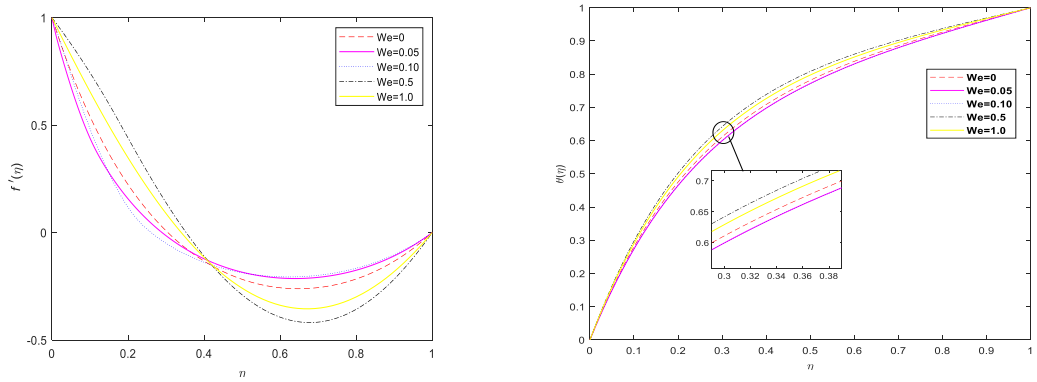

Figure 1 Impact of Williamson parameter We on the (a) velocity $f'(\eta)$ and (b) temperature $\theta(\eta)$ profiles.

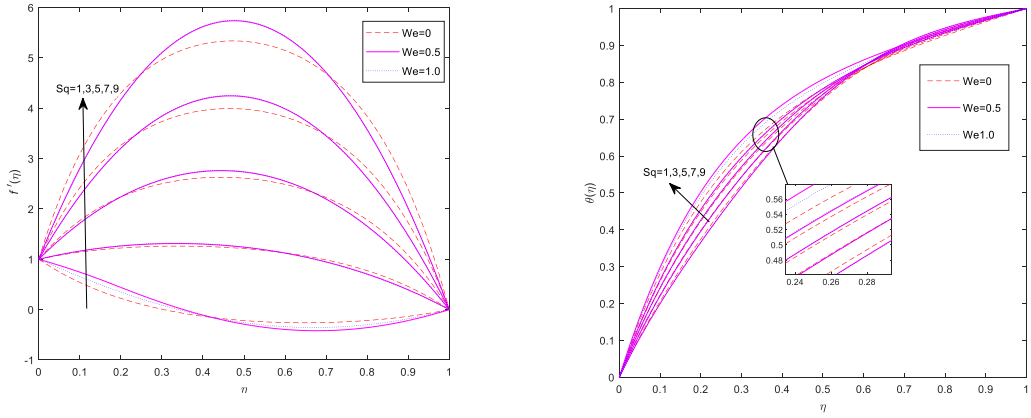

Figure 2 Impact of squeezing parameter Sq on the (a) velocity $f'(\eta)$ and (b) temperature $\theta(\eta)$ profiles.

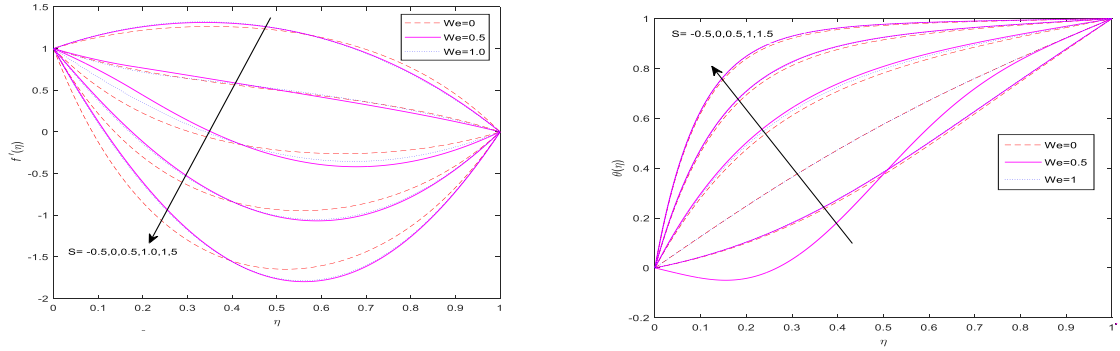

Figure 3 Impact of suction/injection parameter S on the (a) velocity $f'(\eta)$ and (b) temperature $\theta(\eta)$ profiles.

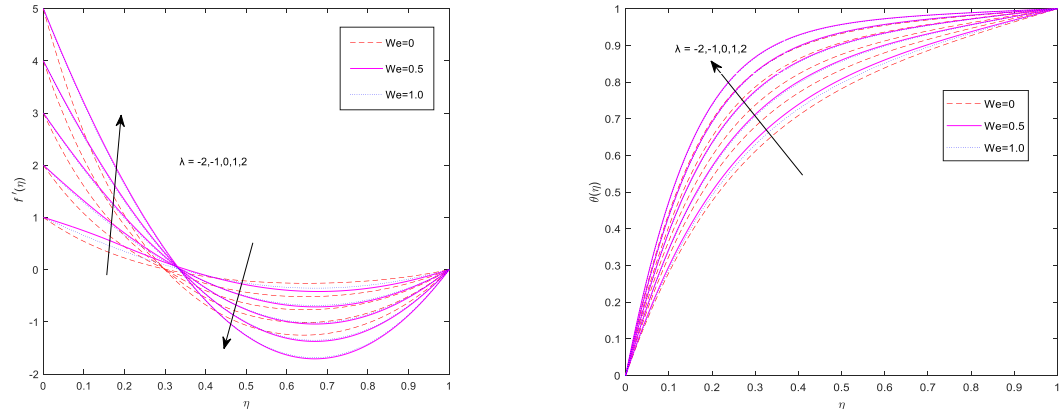

Figure 4 Impact of stretching/shrinking parameter λ on the (a) velocity $f'(\eta)$ and (b) temperature $\theta(\eta)$ profiles.

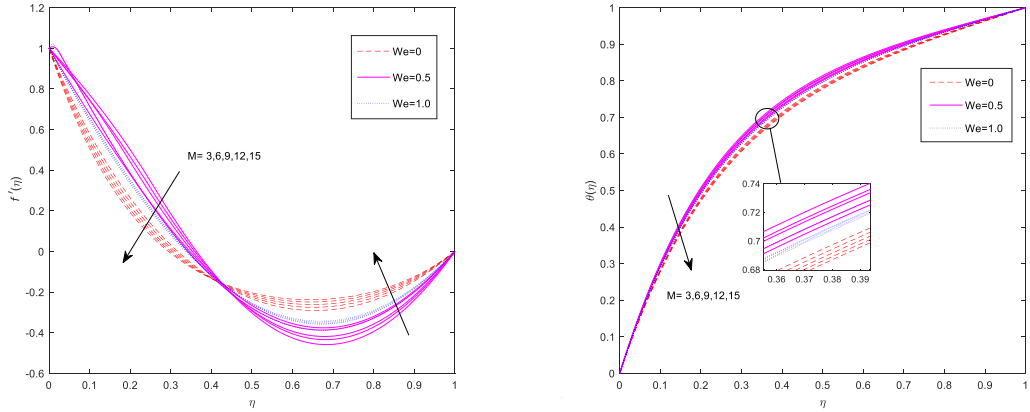

Figure 5 Impact of magnetic parameter M on the (a) velocity $f'(\eta)$ and (b) temperature $\theta(\eta)$ profiles.

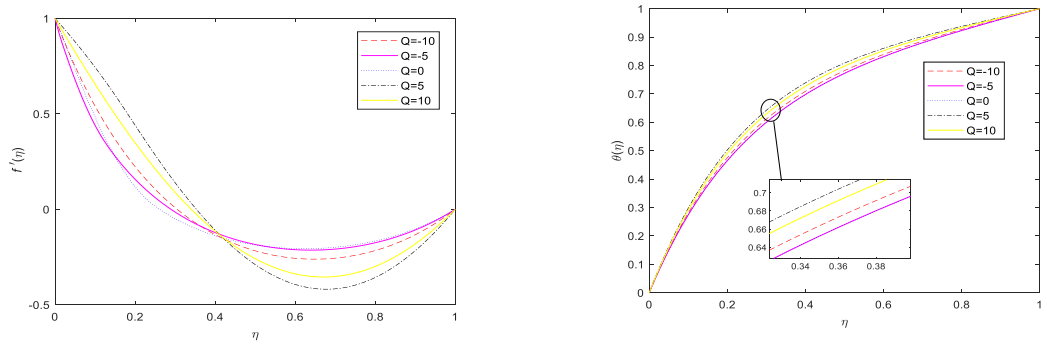

Figure 6 Impact of heat source/sink parameter Q on the (a) velocity $f'(\eta)$ and (b) temperature $\theta(\eta)$ profile

4.2 Skin Friction Coefficient and Nusselt Number

The fluid flow research focused on the effects of squeezing number Sq, suction/injection parameter S, stretching/shrinking parameter λ, magnetic parameter M, heat source/sink parameter Q, Williamson Parameter W, and nanoparticles concentration, ϕ_1 and ϕ_2 . In non-Newtonian fluid

flow, important dimensionless parameter is discussed such as Nusselt number and skin friction coefficient. Skin friction coefficient, C is defined by the shear stress present at the boundary layer of the upper plates and lower plates whereas Nusselt number, Nu is the transfer of heat conductivity across the boundary layer. Both parameters have a significant influence on the non-Newtonian fluid behaviour such as the thermal properties, viscosity of fluid and characteristics flow. Effects of parameters involved on the skin friction and Nusselt number in the context of squeezing flow between two parallel plates is discussed.

Table 4
Numerical values of skin friction coefficients and Nusselt number with various values of physical parameters

Sq	S	λ	M	We	Q	ϕ_1	ϕ_2	$Cf_{x1}Re_x^{\frac{1}{2}}$	$Cf_{x2}Re_x^{\frac{1}{2}}$	$N_{u_x}Re_{x1}^{-\frac{1}{2}}$	$N_{u_x}Re_{x2}^{-\frac{1}{2}}$
	0.1	1	1	1.0	0.5	0.01	0.01	0.8999883	-0.1998140	1.6112575	0.6563294
								3.2658528	8.6652738	1.5379458	0.6088019
								23.9077016	35.5392321	1.4530431	0.5737325
	0.2							0.8388668	0.5997330	2.0366484	0.5405801
	0.3	-1.5						59.6791375	13.4033251	1.1648232	0.9749895
		0						2.7267240	0.2517128	1.8720213	0.6544418
		1	5					7.2258910	1.1912840	2.4016912	0.4828620
			10					1.1654965	3.7110394	2.5703035	0.4277146
			1	1				4.1888767	1.6711733	2.4404305	0.4693726
				0.5				0.0036010	1.8354221	2.4850195	0.4529105
				0	1			-3.2065852	0.607390	2.4010882	0.4848358
				1.0	1.5			4.1888767	1.6711733	2.4404305	0.4693726
					0.5	0.1	0.1	2.2994030	.99409 92	3.0644002	1.1594675
						0.2	0.2	15.4761175	5.8811160	4.2425753	2.3713434

5. Conclusion

This paper studied the magnetic field and heat generation effects on the squeezing Williamson hybrid nanofluid between two parallel plates. This problem transformed dimensionless PDEs into ODEs by using similarity transformation and is modelled using continuity, momentum and energy equations. MATLAB's bvp4c algorithm is used to model the numerical results obtained and are validated by comparing it with published data to show notable agreement. The impact of various physical parameters on velocity profile, temperature profile, skin friction coefficient, and Nusselt number are graphically visualized. The significant findings of this study are as follows:

(i) When squeezing parameter Sq and heat source/sink parameter Q increase, it will increase velocity of fluid while it is observed that fluid velocity is reduced when suction/injection parameter S and magnetic parameter M is increased.

(ii) Increase in the value of S, λ, M and Q will increase the temperature profile which increasing values of Sq and We will lead to the decrease in temperature profile.

(iii) When Lorentz force increase, it causes reduction in velocity near the flow region hence thickness of the momentum boundary layer will increase which causes rise in temperature.

(iv) As We increases, fluid velocity will increase due to thinner velocity boundary layers and more efficient flow. Hence, it will cause decrease in temperature since less energy is stored elastically.

(v) Increase in Sq, S and Q will increase C_{fx} due to the stronger compression between plates which leads to enhanced shear stress.

(vi) When increase in the value of λ and We, C_{fx} will decrease from the greater internal resistance and the stronger flow near the wall.

(vii) As We, λ, M and Q increase, Nu_x will increase due to the less resistant to shear, and more dynamic nanoparticle motion which enhances thermal distribution.

Acknowledgement
The author would like to thank all people who have given unwavering support for the completion of this proceeding.

References

[1] Choi, S. U. S., & Eastman, J. A. (1995). *Enhancing thermal conductivity of fluids with nanoparticles* (No. ANL/MSD/CP-84938; CONF-951135–29). Argonne National Lab. https://doi.org/10.2172/196525

[2] Williamson, R. V. (1929). The flow of pseudoplastic materials. *Industrial & Engineering Chemistry*, 21(11), 1108–1111. https://doi.org/10.1021/ie50239a022

[3] Hayat, T., & Nadeem, S. (2012). Peristaltic transport of a Williamson fluid in an asymmetric channel. *International Journal of Heat and Mass Transfer*, 55(7–8), 1817–1823. https://doi.org/10.1016/j.ijheatmasstransfer.2011.11.040

[4] Buongiorno, J. (2006). Convective transport in nanofluids. *Journal of Heat Transfer*, 128(3), 240–250.https://doi.org/10.1115/1.2150834

[5] Khan, W. A., & Pop, I. (2010). Boundary-layer flow of a nanofluid past a stretching sheet. *International Journal of Heat and Mass Transfer*, 53(11–12), 2477–2483. https://doi.org/10.1016/j.ijheatmasstransfer.2010.01.032

[6] Sheikholeslami, M., & Ganji, D. D. (2016). *Heat transfer in a magnetic nanofluid*. Springer. https://doi.org/10.1007/978-3-319-21864-7

[7] Ellahi, R., Zeeshan, A., & Nadeem, S. (2015). Heat transfer enhancement with Williamson fluid model for blood flow through a tapered stenosed artery. *Applied Mathematics and Computation*, 257, 533–544. https://doi.org/10.1016/j.amc.2014.11.056

[8] Nadeem, S., Mehmood, Z., & Akbar, N. S. (2013). MHD three-dimensional boundary layer flow of a Williamson fluid. *Journal of Magnetism and Magnetic Materials*, 336, 219–224. https://doi.org/10.1016/j.jmmm.2013.03.005

[9] Rashidi, M. M., Kavyani, N., & Abelman, S. (2014). Investigation of entropy generation in MHD and slip flow over a rotating porous disk with viscous dissipation and Ohmic heating. *Energy*,

72, 441–455. https://doi.org/10.1016/j.energy.2014.05.054

[10] Makinde, O. D., & Aziz, A. (2010). Boundary layer flow of a nanofluid past a stretching sheet with a convective boundary condition. *International Journal of Thermal Sciences*, 49(9), 1813–1820. https://doi.org/10.1016/j.ijthermalsci.2010.05.017

[11] Yaseen, M., Rawat, S. K., Shafiq, A., Kumar, M., & Nonlaopon, K. (2022). Analysis of heat transfer of mono and hybrid nanofluid flow between two parallel plates in a Darcy porous medium with thermal radiation and heat generation/absorption. *Symmetry*, 14(9), 1843. https://doi.org/10.3390/sym14091843

[12] Khashi'ie, N. S., Waini, I., Arifin, N. M., & Pop, I. (2021). Unsteady squeezing flow of Cu–Al_2O_3/water hybrid nanofluid in a horizontal channel with magnetic field. *Scientific Reports*, 11, 14128. https://doi.org/10.1038/s41598-021-93692-9

[13] Yasmin, H., Al-Eessa, L. A., Lone, S. A., Raizah, Z., Anwar, S., & Saeed, A. (2024). A numerical framework of magneto Williamson hybrid nanofluid over a porous sheet: A classical Keller box analysis. *Results in Physics*, 59, 107552. https://doi.org/10.1016/j.rinp.2023.107552

[14] Chambers, D. W., Baglivo, J. A., Ebel, J. E., & Kafka, A. L. (2012). Earthquake forecasting using hidden Markov models. *Pure and Applied Geophysics*, 169, 625–639. https://doi.org/10.1007/s00024-011-0337-4

[15] Abbas, W., Megahed, A. M., Ibrahim, M. A., & Said, A. A. (2023). Ohmic dissipation impact on flow of Casson-Williamson fluid over a slippery surface through a porous medium. *Indian Journal of Physics*, 97(14), 4277–4283. https://doi.org/10.1007/s12648-023-02501-y

[16] Sankari, S., Rao, M. E., Elsiddieg, A. M., Khan, W., Makinde, O. D., Saidani, T., **et al.** (2025). Analytical solution of MHD bioconvection Williamson nanofluid flow over an exponentially stretching sheet with the impact of viscous dissipation and gyrotactic microorganisms. *PLoS ONE*, 20(3), e0306358. https://doi.org/10.1371/journal.pone.0306358